^{124}I PET-based 3D-RD dosimetry for a pediatric thyroid cancer patient: real-time treatment planning and methodological comparison

Robert F Hobbs, Richard L Wahl, Martin A Lodge, Mehrbod S Javadi, Steve Y Cho, David T Chien, Marge E Ewertz, Caroline E Esaias, Paul W Ladenson, George Sgouros.

Johns Hopkins University, Baltimore MD 21231, USA

SI. MATERIALS AND METHODS

Data acquisition

The quantity of activity was chosen as an optimal compromise between imaging quality and the concern over a possible stunning effect. Whole body scans (10 bed positions; 6 min per position) were acquired on a Discovery RX PET/CT system (GE Healthcare; Waukesha, WI) in 2D mode at 1, 24, 48, 72, and 96 h after tracer administration. Blood samples were drawn concurrently at 1, 4, 24, 48, 72, and 96 h and counted in an ^{124}I calibrated gamma counter. Aside from avoiding the effects of previously administered ^{131}I, the greater sensitivity, higher resolution, and reduced scatter of ^{124}I PET provided an advantage in terms of accuracy over ^{131}I SPECT in the 3D-RD dosimetry calculations.

Activity quantification was based on an ^{124}I standard measurement in the dose calibrator and imaging of the same standard on the PET/CT in 2D mode. All patient and standard data were acquired with the tungsten septa in place (0.8 mm thick, 54 mm long), so as to minimize false coincidence counts from cascade gamma rays.

Real-time 3D-RD calculation

A more complete description of 3D-RD has been previously provided (*1*). In the real-time implementation, a dose-rate map was generated as each image was acquired. After importing each image into 3D-RD and correcting for the difference in ^{131}I vs ^{124}I half-lives the following procedure was followed:

1. Using the Electron Gamma Shower (EGS) Monte Carlo (MC) software, one million events were run for the electron and photon components of the ^{131}I decay spectra, for each time point (electron and photon spectra probability distributions obtained from LBL/Lund web site (*2*)).

2. A volume of interest (VOI) contour was manually drawn around the lungs using the CT from the first PET/CT scan.

3. After acquiring the data and creating a map of the deposited energy from MC for each time point, these maps were loaded back into a HERMES (HERMES Medical Solutions; Stockholm, Sweden) workstation for CT-based registration.

4. The registered energy deposition distributions were returned to 3D-RD where they were weighted according to temission-type probability for ^{131}I and unit activity and converted to absorbed dose rate valuesfor the entire lung VOI and the individual voxels.

5. The dose rates for the lung VOI (as defined in item 2) were fit with a formula analogous to Equation (S1), below, and the area under the curve calculated as the absorbed dose per unit activity.

6. The administered activity was scaled from unit activity to administer 27 Gy (*3*) to the lung VOI, calculated as a whole.

OLINDA/whole-organ S-value-based calculation

The first 4 PET activity images were registered over time to each other via their respective CTs on the HERMES workstation using the built-in mutual information based registration software, and the VOI drawn on the first scan was applied to each image. Using the co-registered PET activity images, the counts within the lung VOI were taken and converted to activity, corrected for ^{124}I to ^{131}I conversion, and fit with an activity curve of the form:

$$A(t) = A_0(1 - e^{-\kappa t})e^{-\lambda t}, \qquad \text{(S1)}$$

which allows for a short period of activity uptake, followed by exponential decay. Here κ is the activity uptake constant, λ is the clearance rate constant, and A_0 characterizes the order of magnitude of the activity. The residence time is obtained by dividing the cumulated activity (the integral of the activity) by the administered activity.

The remainder whole body residence time was obtained in a similar fashion using the whole-body PET images. The total counts minus the counts in the lungs and brain tumors were considered and converted to activity. The brain tumor activities were excluded as they were considered large but remote to the lungs. The remainder whole body curve was fit with the function:

$$A(t) = A_1 e^{-\lambda_1 t} + A_2 e^{-\lambda_2 t} \qquad \text{(S2)}$$

where λ_1 and λ_2 are clearance rate constants (one rapid, one longer-lived) and A_1 and A_2 are the contributions from each mode to the initial activity.

The two residence times were input into OLINDA for all ORNL (Christy-Eckerman) phantoms (*4*). The absorbed dose per unit activity results, *D*, were fit with a power function, $D = am^b$, where *m* is the phantom mass. The patient's mass (37 kg) was input into the equation to obtain the patient absorbed dose per unit activity from which the administered activity necessary to deliver the 27 Gy maximum tolerated dose (*3*) to the lungs was obtained.

Benua-Leeper calculation

The total body activity, *A*, including all tumors was measured for the 4 different time points using the PET images and fit to a double exponential (Equation S2). The value A(48 h) was calculated from the functional fit and scaled to a value of 2.96 GBq (80 mCi) for therapeutic ^{131}I (*5*). This scaling factor was applied to the diagnostic administered activity to obtain the predicted therapeutic ^{131}I activity necessary to obtain the limiting whole body activity at 48 h. The absorbed dose to blood was also calculated to set a limit on bone marrow toxicity from the counted blood samples using standard methodology.

Retrospective 3D-RD analysis

A retrospective analysis of tumor absorbed dose from the same diagnostic data was performed using 3D-RD after completion of the real-time calculation of the therapeutic ^{131}I. In the retrospective calculation, other regions of interest were considered as well, including the two brain metastases, a lymph node near the sternum, and the thyroid bed. The absorbed dose was calculated for all VOIs and the 3D-RD analysis included BED and EUD calculations as well as dose volume histograms (DVHs) for a voxelized interpretation of the results. BED is intended to account for the biological effects of different dose-rates (i.e., clearance kinetics) and is defined as (*6*):

$$BED = D\left(1 + \frac{G(\infty)}{\alpha/\beta} \cdot D\right) \tag{S3}$$

Where α and β are the radiobiological parameters from the linear quadratic equation (*7*), *D* is the absorbed dose, and *G(T)* is the Lea-Catcheside G-factor (*8*), which depends on μ, the DNA repair rate. For all VOIs and VOI voxels the BED was calculated numerically (*9*).

The EUD accounts for the biological effects of a non-uniform dose distribution and is calculated using the formula (*10*):

$$EUD = -\frac{1}{\alpha}\ln\left(\sum_{i=1}^{N}\frac{e^{-\alpha BED_i}}{N}\right) \tag{S4}$$

where *N* is the number of voxels and BED_i are the individual voxel BED values. The values used for the radiobiological parameters are taken from the literature (*11-13*) and are shown in Table SI.

Table SI. Radiobiological parameters used in 3D-RD.

Tissue	α (Gy^{-1})	β (Gy^{-2})	μ (h^{-1})
Lung	0.0172	0.00521	0.46
Tumor	0.365	0.028	1.3

Except for the lungs, the tumor sites were considered small enough to be affected by the partial volume effect (PVE). Accordingly, the activity concentration values were adjusted with volume-based recovery coefficients (RCs) taken from the literature (*14*) for similar field width at half maximum (FWHM) collimator values. The VOIs were all drawn on a CT co-registered to the PETs and dose maps.

The voxel dose rate curves could not be fit to a single mathematical expression, they were defined piece-wise: trapezoids were fit between the different time points and an exponential function was used to extrapolate beyond the last time point, the clearance rate used in this function was either the clearance rate of the exponential calculated between the last three time points, or, if this latter was longer than physical decay, the physical decay rate of ^{131}I was used.

Lung Dosimetry

An attempt was made to distinguish normal lung tissue from tumor in the lung VOI based on data from the voxelized results. In actual fact, most voxels are likely a combination of tumor and normal lung tissue as the individual metasteses are smaller than the voxel size and certainly not of voxel shape and difficult to detect individually (*15*). A satisfactory definition of normal lung tissue and tumor tissue in the lung VOI is necessary for voxelized BED and EUD results, as the radiobiological parameters depend strongly on the type of tissue. The most important clinical consideration is a reliable determination of normal lung for purposes of lung toxicity evaluation. Of the several options considered, the most relevant criterion for tissue type distinction appeared to be segmentation based on activity uptake at 24 h; voxels with activity > 30 mBq/voxel (voxel volume = $7.19\ 10^{-2}$ ml) were considered tumor, the rest normal lung tissue. Discrimination by density, determined by converting CT values, as used in a previous 3D-RD calculation (*1*) and clearance rate (*16*) did not provide as good and consistent a tumor delineation although there was a great degree of overlap between all the approaches considered.

Normal Brain Dosimetry

Also of concern was the potential toxicity to the brain surrounding the tumor metastases, in particular, the tissue in close proximity to the left temporal lobe lesion, which showed extraordinarily high uptake and caused local reconstruction artifacts (Figure 1b). Even in the absence of such artifacts, count rate spill-over outside the defined tumor volume due to the partial volume effect would give artificially high absorbed dose values to normal brain. In order to accurately estimate the dose to normal brain tissue, the spatial distribution of activity as represented in the PET images was not used directly in the 3D-RD calculation for normal brain, rather average activity concentrations were assigned to tumor and normal brain as delineated on the CT portion of the PET/CT scan. This hybrid approach, using VOIs to obtain activity concentration that was then uniformly assigned to CT-defined anatomical volumes, made it possible to assign cumulated activity equal to the average tumor cumulated activity in each voxel of the anatomically defined tumors with the average background cumulated activity placed in the normal brain tissue. One million MC events were run; the energy deposition was scaled to the total cumulated activity, collected into voxels, and converted to absorbed dose.

Benual-Leeper Dose rate constraint (DRC) method

The Benua-Leeper method was established from data from a series of 15 patients in the 1950's, essentially adults. It does not allow for patient size variability which may be extreme, especially if one considers pediatric patients. A method exists that adapts the 80 mCi rule at 48 h (*5*) to a dose rate constraint (DRC) that is dependent on the phantom used and the percentage of the whole body activity retained in the lungs at 48 h (*17*). This approach makes it possible to translate the 80 mCi constraint to pediatric cases. The approach essentially converts 80 mCi in the lungs for the adult phantom to a dose-rate constraint. The resulting dose-rate constraint is them assumed to apply to pediatric phantoms and is used in conjunction with the pediatric phantom to derive the corresponding administered activity constraint. A complete description is provided in the literature (*17*), briefly:

$$DRC = A_T \cdot F_T \cdot S^P_{LU \leftarrow LU} + A_T \cdot (1 - F_T) \cdot S^P_{LU \leftarrow RB} \qquad \text{(S5)}$$

where A_T is the whole body activity at time T (48 h), F_T is the fraction of A_T present in the lungs at 48 h and S are the S-values for a specific phantom, *P*, for lung to lung (LU←LU) and for rest of body (whole body excluding the lung) to lung (LU←RB). This last quantity is derived from the formula:

$$S^P_{LU \leftarrow RB} = S^P_{LU \leftarrow TB} \cdot \frac{M^P_{TB}}{\left(M^P_{TB} - M^P_{LU}\right)} - S^P_{LU \leftarrow LU} \cdot \frac{M^P_{LU}}{\left(M^P_{TB} - M^P_{LU}\right)} \qquad \text{(S6)}$$

where *S(LU←TB)* is the total body to lung S-factor, the *M*s are the total body and lung masses for phantom *P*. The assumption in the model was that the 80 mCi (A_T = 2.96 GBq) rule was established from data most closely approximating the adult female phantom (*P*) with 90% activity retention in the lungs (F_T). The adult female S-values were therefore used to calculate the DRC. By solving for A_T in Equation (S5), renamed A^P_{DRC}, the maximum activity retained at 48 h based on the DRC for the *P* phantom, the expression becomes:

$$A^P_{DRC} = \frac{DRC}{F_{48} \cdot S^P_{LU \leftarrow LU} + (1 - F_{48}) \cdot S^P_{LU \leftarrow RB}} \qquad \text{(S7)}$$

where the S-values are now those for the phantom of interest and F_{48} is the patient's fraction of activity in the lungs at 48 h. The activities from Equation (S7) for all ORNL (Christy-Eckerman) phantoms are plotted as a function of phantom mass, *m*, and fit with a linear equation A = am+b. The mass of the patient is used into the fit equation and the resulting activity constraint at 48 h was obtained. The administrated activity necessary to obtain such a constraint (AA_{max}) was calculated by scaling the measured 48 h unit activity to the values obtained in Equation (S7) as specified by the standard Benua-Leeper method.

SII. RESULTS

Real-Time 3D-RD calculation

The dose calculated from integrating the fit to the dose rates from the diagnostic activity (analogous to Equation S1) gave 199 mGy for 37 MBq (1 mCi) of ^{131}I. The scaled administered activity predicted to deliver 27 Gy to the lung VOI, considered as a whole, was 5.11 GBq (138 mCi) of ^{131}I.

OLINDA/whole-organ S Value-based calculation

The lung activities were fit to Equation (S1) (A_0 = 22.57 MBq, κ = 0.397 h^{-1}, λ = 6.646 10^{-3} h^{-1}, $R^2 > 0.99$), while the whole body pool activities were fit to Equation (S2) (A_1 = 67.16 MBq, A_2 = 26.44 MBq, λ_1 = 0.106 h^{-1}, λ_2 = 1.36 10^{-2} h^{-1}, $R^2 > 0.99$). By integrating the fits and dividing by the administered activity, residence times of 35.5 h for the lungs and 27.4 h for the remainder of body were obtained. To best approximate the lung to lung S-value for the treated patient, the S-values already tabulated in OLINDA were interpolated by calculating the absorbed doses to the lungs calculated for every phantom plotting the estimated absorbed dose against the whole-body mass of each phantom and then fitting a power law function, $D = am^b$ (a = 225 mGy/MBq-kg, b = -0.9045, $R^2 > 0.99$) to the data. For the patient with a whole body mass of 37 kg this translates to an absorbed dose of 8.59 mGy/MBq, giving 3.14 GBq (85 mCi) of administered activity to deliver 27 Gy to the lungs considered as a whole (*i.e.*, including tumor).

Benua-Leeper Calculation

The resultant fit parameters to Equation (S2) using the whole body activities used to calculate the Benua-Leeper maximum administered activity are: A_1 = 53.62 MBq, A_2 = 41.26 MBq, λ_1 = 6.21 10^{-2} h^{-1}, λ_2 = 5.74 10^{-3} h^{-1}, $R^2 > 99$. The total body activity at 48 h calculated using the functional fit, for 94 MBq of administered ^{131}I, is 34.05 MBq. Scaling this value to 2.96 GBq (80 mCi) gave a recommended administered activity of 8.17 GBq (220 mCi). The bone marrow toxicity constraint, calculated from a limit of 2 Gy to blood was 5.60 GBq (151 mCi).

Retrospective 3D-RD tumor lesion dosimetry

After the real-time calculations were completed and the results provided to the treating physician, the 3D-RD dosimetry calculations were expanded to examine tumor absorbed dose. The left and right brain tumors and the thyroid bed dose rate values were plotted and fit to a functional form similar to that used for the lungs (analogous to Equation S1). The suprasternal tumor therapeutic dose rates were fit to a simple exponential with a constraint of physical decay (λ_φ) on the clearance rate. The PVE RCs for the activity in the VOIs were 0.6 for the left brain tumor, 0.5 for the thyroid bed and 0.3 for the right brain tumor and the suprasternal tumor. The fit parameters for the therapeutic quantities to the lungs and tumors are given in Table SII.

Table SII. Fit parameters to the therapeutic dose rate functions for the different VOIs. The suprasternal tumor is fit to a simple exponential function, all others are fit to an uptake function analogous to Eq. (S1).

Parameters	Lung	L Brain	R Brain	Suprasternal	Thyroid bed

		tumor	tumor	tumor	
$\dot{D}_0$ (Gy/h)	0.186	4.08	0.751	0.110	0.518
κ (h^{-1})	0.436	0.108	0.230	-	0.691
λ (h^{-1})	$6.68\ 10^{-3}$	$4.00\ 10^{-3}$	$5.19\ 10^{-3}$	$\lambda_\varphi = 3.61\ 10^{-3}$	$1.51\ 10^{-2}$
R^2	> 0.99	0.97	0.98	0.64	0.94

Retrospective 3D-RD normal lung and lung tumor dosimetry

The activity concentration-based criterion for segmenting normal lungs vs. tumor tissue in the lungs was applied to identify tumor vs. normal lung tissue voxels. Voxels identified as tumor in this manner are shown, superimposed upon coronal CT image slices, in Figure S1. The images are different from Figure 1b in that all activity in the lung voxels corresponding to normal lung tissue have been set to zero leaving only the voxels defined as tumor showing uptake. Also the matrix size of the CTs have been modified to conform to the matrix size of the PET, from 512x512 to 128x128, as this was the matrix size used in the analysis. Figure S2A shows the dose volume histograms (DVHs) for the two tissue types and Figure S2B shows the BED histograms.

Fig. S1

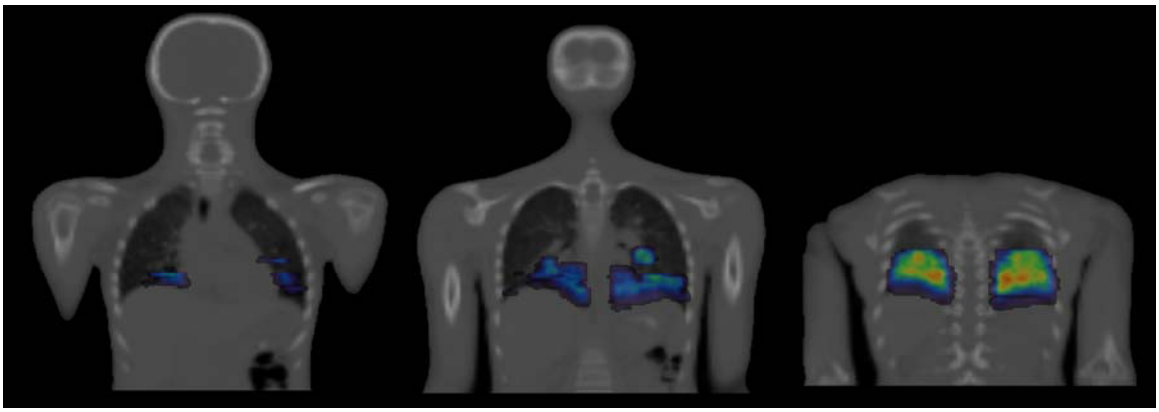

Figure S1. Selected coronal views of the cumulated activity maps of the lungs fused with CT. Results of the lung tumor segmentation are shown by setting to zero all activity voxels not identified as tumor. The views extend from the lower torso to the vertex of the skull.

Fig.S 2

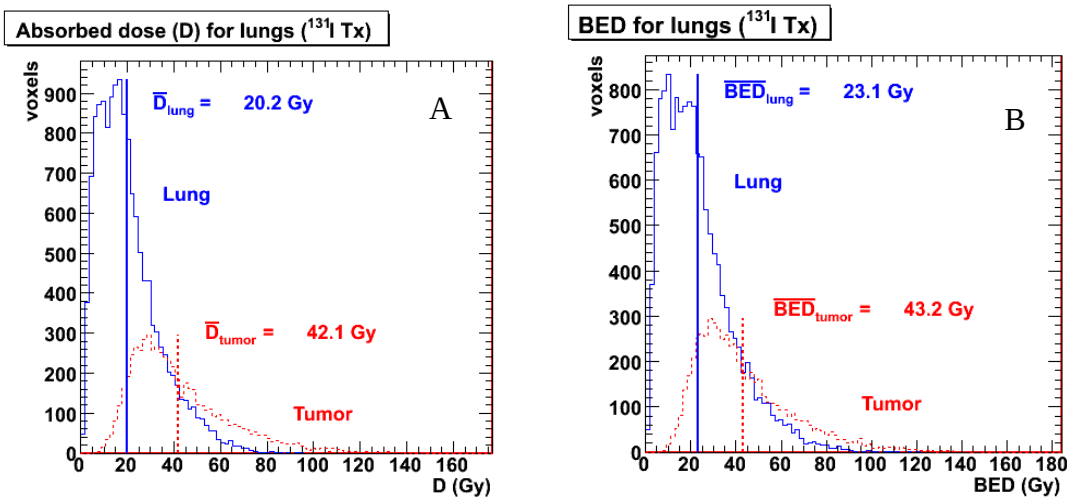

Figure S2. Dose volume histograms (and BED histograms) for the lung VOI voxels. The blue histograms represent normal lung tissue, while the red lines are tumor tissue. The thick vertical lines show the voxel averages.

3D-RD, model-based normal brain dosimetry

The brain model with high cumulated activity confined to the tumor volumes as defined on the CT and background cumulated activity in the normal brain tissue gave a maximum absorbed dose in a single voxel of 65.6 Gy, while the average absorbed dose was 0.95 Gy. Only 9 voxels (out of 76437, i.e. 0.012 %) had doses greater than 50 Gy, and only 101 (0.13 %) had doses greater than 20 Gy.

Re-evaluation of the OLINDA method

A search for the discrepancy between the S-value-based/OLINDA calculation and 3D-RD results revealed an important difference in mass between the patient's lungs and the reference mass used in OLINDA (453 g for the 10-year old phantom and 651 g for the 15-year old phantom). The patient has a denser lung than typical due to the extent of disease (~ 0.56 g/ml) for a total of 822 g lung mass, determined by converting the voxelized CT values. Absorbed dose is energy absorbed divided by mass; by increasing the mass in the lungs, the dose is decreased, therefore more activity is required to reach the limiting absorbed dose. By plotting and fitting the absorbed dose, *D*, for each phantom versus lung mass, m_l, rather than WB mass, inputting the patient's lung mass and repeating the OLINDA calculation with the new lung mass-based fit $D = am_l^b$ (a = 3.633 mGy/MBq-kg, b = -0.9727, $R^2 > 0.99$), a recommended value of 5.17 GBq is obtained: a value much more in agreement with the 3D-RD value. Alternatively, by using the OLINDA option of adjusting the mass of the lungs to the measured value and repeating the calculation, a recommended value of 5.36 GBq is obtained (regardless of the choice of phantom), also much more aligned with the 3D-RD value.

Re-evaluation of the Benua-Leeper Method

Similarly, adjusting the 80 mCi limit by applying the DRC method yielded results closer to 3D-RD. The DRC calculated from Equation (S5) was 22.1 cGy/h, using the S-values for the female phantom and $F_T = 0.90$. Inserting the DRC value, the S-values for the

various phantoms, and a measured $F_{48} = 0.48$ from the patient into Equation (S7) and fitting the output resulted in "80 mCi rule"-equivalent constraint of 1.87 GBq for the patient. For this activity to be present at 48 h, considering that 35.1 MBq was retained for 94 MBq of administered ^{131}I, required an administered activity of 5.16 GBq. This administered activity is substantially less than the 8.17 GBq obtained with the unmodified B-L method and also below the 5.60 GBq amount that would yield 2 Gy to blood.

SIII. DISCUSSION

Post-therapy results

Given the available imaging resolution, discrimination between normal tissue and lung tissue is difficult if not impossible and can only give an idea of the delineation for what are most likely micro-metastases smaller than the resolution of the detector (*15*). The average difference between the BED of the two tissue types (Figure S2b) is less than the average difference of the absorbed doses (Figure S2a) because of the greater values for α/β and μ (*i.e.*, because of the greater radioresistance) of tumor over normal lung tissue (Table SI), which more than compensates for the quadratic effect of the BED (Equation S3). Similarly, the great difference in α values explains the greater EUD to BED difference in the tumor tissue. Because of this mix of tissue types, no BED was calculated for the lung VOI as a whole, as the radiobiological parameter values are only valid for a specific tissue type.

The EUD values have a much smaller range than the BED or absorbed dose values. In particular, the EUD for the left brain tumor is only ~2x that of the right brain tumor. This reflects the nature of the EUD: for very small values of BED (~ mGy), the EUD is typically the average of the BED values, while for large BED values, as is the case for the left brain tumor, the EUD is dominated by the smallest values in the distribution. From a practical standpoint this means that the EUD is essentially determined by the low values of the voxels on the edges of the VOI. These voxels are especially susceptible to artificial variations due to seemingly minor effects of miss-registration and re-distribution of activity counts from PVE spill-off on the borders of the tumor site. The root mean square (RMS), which quantifies the spread of values in a distribution, of the BED voxel values for the left brain tumor as measured from the activity images is 1020 Gy; while for the homogenous cumulated activity model of the left brain tumor, for a same average BED (1220 Gy) the RMS is only 47 Gy. Consequent to this lesser spread of BED values, the EUD for the modeled brain tumor is 1023 Gy, while the image-based EUD calculation gives a value of 89 Gy (Table I). This last value is clearly affected by the large spread, in particular by the extreme lower end of the distribution.

The average dose to brain tissue as shown in the brain model is relatively small, but the maximum voxel absorbed dose is 65.6 Gy. This value is slightly above the generally accepted 50-60 Gy threshold for gray matter toxicity (*18*), while the vast majority of voxels are significantly lower.

The focus of this study was treatment planning rather than general tumor dosimetry, for which a few additional methodological steps could have been implemented. In particular, the accuracy of the dosimetry for the small tumor sites would be improved by a more rigorous determination of PVE values specific to the isotope and camera used for the data acquisition. The literature values are all based on ^{18}F rather than ^{124}I, however, there exists reasonable evidence that acquisition in 2D mode with septa in place minimizes the false coincidences from cascade gammas and does not affect the PVE RCs substantially (*19*). The large initial positron energy from ^{124}I decays modifies the expected PVE RCs slightly (*19*). A slightly different PVE RC curve could be expected on a the camera used for analysis, as opposed to the literature-based values, however the uncertainty is likely less than the degree of precision generally given to PVE RC values (one significant figure). An additional uncertainty exists for the left brain tumor given the high uptake and the noticeable repercussions (artifacts seen in Figure 1b) on the image quality and the quantification whose resolution would require extensive extra effort.

References

1. Prideaux AR, Song H, Hobbs RF, He B, Frey EC, Ladenson PW, Wahl RL, Sgouros G. Three-dimensional radiobiologic dosimetry: application of radiobiologic modeling to patient-specific 3-dimensional imaging-based internal dosimetry. *J Nucl Med.* Jun 2007;48(6):1008-1016.

2. Ekström L, Firestone R. WWW Table of Radioactive Isotopes. http://ie.lbl.gov/toi/index.htm.

3. Press OW, Eary JF, Appelbaum FR, Martin PJ, Badger CC, Nelp WB, Glenn S, Butchko G, Fisher D, Porter B, et al. Radiolabeled-antibody therapy of B-cell lymphoma with autologous bone marrow support. *N Engl J Med.* Oct 21 1993;329(17):1219-1224.

4. Christy R, Eckerman K. *Specific absorbed fractions of energy at various ages for internal photon sources.* Oak Ridge, TN: Oak Ridge National Laboratory; 1987.

5. Benua R, Leeper R. A method and rationale for treating metastatic thyroid carcinoma with the largest safe dose of ^{131}I. In: Medeiros-Neta G, E G, eds. *Frontiers in Thyroidology*. New York, NY: Plenum Medical; 1986:1317-1321.

6. Dale RG. The application of the linear-quadratic dose-effect equation to fractionated and protracted radiotherapy. *Br J Radiol.* Jun 1985;58(690):515-528.

7. Fowler JF. The linear-quadratic formula and progress in fractionated radiotherapy. *Br J Radiol.* Aug 1989;62(740):679-694.

8. Millar WT. Application of the linear-quadratic model with incomplete repair to radionuclide directed therapy. *Br J Radiol.* Mar 1991;64(759):242-251.

9. Hobbs RF, Sgouros G. Calculation of the Biological Effective Dose (BED) for Piece-Wise Defined Dose-Rate Fits. *Med Phys.* 2009;36(3):904-907.

10. Niemierko A. Reporting and analyzing dose distributions: a concept of equivalent uniform dose. *Med Phys.* Jan 1997;24(1):103-110.

11. Van Dyk J, Mah K, Keane TJ. Radiation-induced lung damage: dose-time-fractionation considerations. *Radiother Oncol.* Jan 1989;14(1):55-69.

12. Challeton C, Branea F, Schlumberger M, Gaillard N, de Vathaire F, Badie C, Antonini P, Parmentier C. Characterization and radiosensitivity at high or low dose rate of four cell lines derived from human thyroid tumors. *Int J Radiat Oncol Biol Phys.* Jan 1 1997;37(1):163-169.

13. Bodey RK, Flux GD, Evans PM. Combining dosimetry for targeted radionuclide and external beam therapies using the biologically effective dose. *Cancer Biother Radiopharm.* Feb 2003;18(1):89-97.

14. Soret M, Bacharach SL, Buvat I. Partial-volume effect in PET tumor imaging. *J Nucl Med.* Jun 2007;48(6):932-945.

15. Freudenberg LS, Jentzen W, Muller SP, Bockisch A. Disseminated iodine-avid lung metastases in differentiated thyroid cancer: a challenge to 124I PET. *Eur J Nucl Med Mol Imaging.* Mar 2008;35(3):502-508.

16. Kolbert KS, Hamacher KA, Jurcic JG, Scheinberg DA, Larson SM, Sgouros G. Parametric images of antibody pharmacokinetics in Bi213-HuM195 therapy of leukemia. *J Nucl Med.* Jan 2001;42(1):27-32.

17. Sgouros G, Song H, Ladenson PW, Wahl RL. Lung toxicity in radioiodine therapy of thyroid carcinoma: development of a dose-rate method and dosimetric implications of the 80-mCi rule. *J Nucl Med.* Dec 2006;47(12):1977-1984 (Dec 2007:2027).

18. Steen RG, Koury BSM, Granja CI, Xiong X, Wu S, Glass JO, Mulhern RK, Kun LE, Merchant TE. Effect of ionizing radiation on the human brain: white matter and gray matter T1 in pediatric brain tumor patients treated with conformal radiation therapy. *Int J Radiat Oncol Biol Phys.* Jan 1 2001;49(1):79-91.

19. Jentzen W, Weise R, Kupferschlager J, Freudenberg L, Brandau W, Bares R, Burchert W, Bockisch A. Iodine-124 PET dosimetry in differentiated thyroid cancer: recovery coefficient in 2D and 3D modes for PET(/CT) systems. *Eur J Nucl Med Mol Imaging.* Mar 2008;35(3):611-623.